Dalton Transactions

RSC Publishing

PAPER

Zirconium and hafnium complexes based on 2-aryl-8-arylaminoquinoline ligands: synthesis, molecular structure, and catalytic performance in ethylene copolymerization†

Cite this: DOI: 10.1039/c2dt31856c

Ilya E. Nifant'ev,*[a,b] Pavel V. Ivchenko,[a] Vladimir V. Bagrov,[a] Sandor M. Nagy,*[c] Linda N. Winslow,[c] Jean A. Merrick-Mack,[c] Shahram Mihan[d] and Andrei V. Churakov[e]

Received 14th August 2012,
Accepted 26th September 2012

DOI: 10.1039/c2dt31856c

www.rsc.org/dalton

A general and efficient approach toward new zirconium and hafnium complexes based on 2-aryl-8-arylaminoquinoline ligands was developed. These precursors, when activated with MAO/borate cocatalyst and supported on silica, result in active olefin polymerization catalysts. The ethylene copolymers produced under industrially relevant conditions show very high molecular weights and unique microstructures defined by the multisite nature of the catalyst. A site-diversification mechanism is proposed to explain the presence of at least five individual sites, as deduced from 3D-TREF analysis of ethylene–butene copolymers.

Introduction

We continue to witness remarkable progress toward new polyolefins enabled by an increasing number of post-metallocene catalyst precursors based on various chelating-ligand topologies.[1] Selected recent examples of catalyst precursors with various multi-dentate ligands and metal centers are presented in Scheme 1. Phenoxyimine–titanium complexes **A** were shown to be active catalyst precursors capable of sustaining the living polymerization of olefins under certain conditions,[2] whereas bis-imino pyridine complexes of iron **B**, depending on the nature of the aryl substituent, led to a wide range of oligomeric to high-molecular-weight products.[3] Complexes **C**,[4] **D**[5] and **E**[6] further illustrate the fascinating diversity of chelating-ligand environments that support catalytically active sites of respectable activity.

The purpose of the current study is to present a general synthetic approach that leads to a large variety of [CNN] chelate complexes based on the quinoline scaffold **F**, which is structurally related to the popular pyridine-based [CNN] chelate topology **E**[6] (Scheme 1).

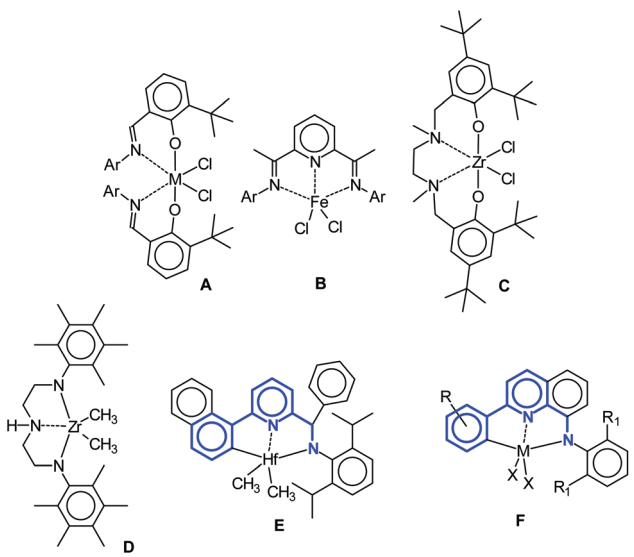

Scheme 1 Post-metallocene catalyst precursors.

The quinoline building block explored in recent studies[7] proved to be a very prolific ligand framework because of the relative ease of independent variation of the substituents in positions 2 and 8 of the quinoline ring systems. These variations generate a wide range of ligand precursors, which, in turn, allows broad control of the electronic and steric

[a]*Department of Chemistry, M. V. Lomonosov Moscow State University, Leninskie Gory, 1-3, Moscow 119991, Russia. E-mail: inif@org.chem.msu.ru*
[b]*A. V. Topchiev Institute of Petrochemical Synthesis RAS, 29 Leninsky Prosp., Moscow 119991, Russia*
[c]*Equistar Chemicals LP, Cincinnati, OH 45249, USA. E-mail: Sandor.Nagy@lyondellbasell.com*
[d]*Basell Polyolefine GmbH, Frankfurt am Main, D-65926, Germany*
[e]*N. S. Kurnakov Institute of General and Inorganic Chemistry RAS, 31 Leninsky Prosp., Moscow, 119991, Russia*

†Electronic supplementary information (ESI) available. CCDC 859965–859967. For ESI and crystallographic data in CIF or other electronic format see DOI: 10.1039/c2dt31856c

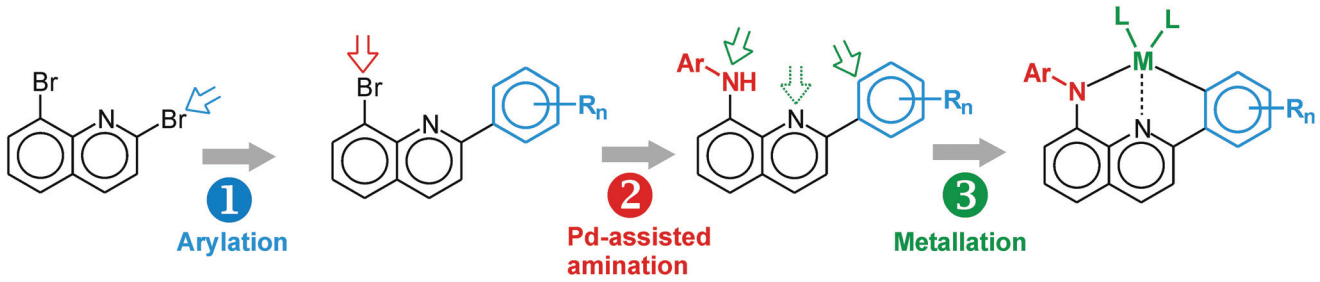

Fig. 1 General synthetic strategy toward complexes **F**.

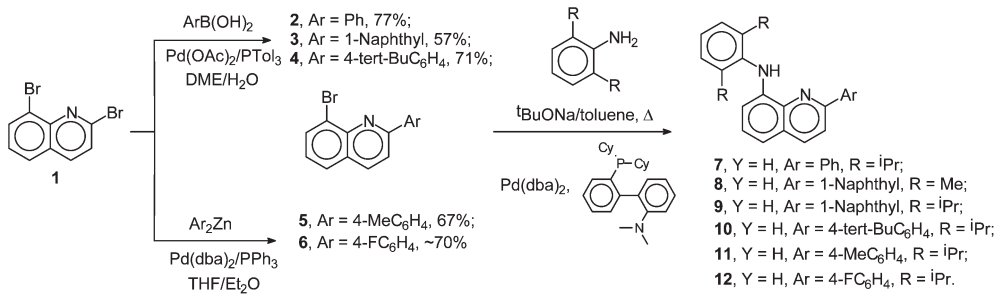

Scheme 2 Preparation of 2-aryl-8-arylaminoquinolines **7–12**.

properties of the inner coordination sphere of the metal center. Recent publications from several groups clearly indicate the rapidly increasing popularity of the quinoline template in the design of next-generation polymerization systems.[7]

Results and discussion

2,8-Dibromoquinoline **1**, which was selected as a convenient starting material for the complexes **F** in this study, can be easily prepared in three steps from 2-bromoaniline using known procedures.[8] The general approach toward the various ligand precursors is based on the significantly different reactivity of bromine atoms attached to the azine *versus* the benzene parts of the ring system – position 2 *vs.* 8 (Fig. 1).

Preparation of quinoline-based CNN-type ligands

The transformation of 2,8-dibromoquinoline **1** into the [CNN]-type ligand precursors were accomplished in two consecutive steps. In the first stage, selective substitution of the bromine atom at position 2 resulted in 2-aryl-8-bromoquinolines **2–6**; subsequent Buchwald–Hartwig amination of these intermediates resulted in the target compounds **7–12** (Scheme 2); this procedure is similar to that previously reported for the synthesis of 2-phenyl-8-phenylaminoquinoline.[8b]

To prepare the intermediates **2–4**, we selected the general Suzuki–Miyaura method[9] and started from commercially available arylboronic acids (Scheme 2) using the $Pd(OAc)_2$/$P(o\text{-tolyl})_3$ catalyst in a two-phase DME/water system.[10] The undesirable need for an excess of arylboronic acids can be avoided through the use of sterically demanding phosphines instead of the traditional PPh_3, which ensures a higher reaction rate and increased selectivity *via* suppression of the hydrolytic deborylation side reaction.[10e]

An alternative method to prepare the bi-aryls is the Negishi cross-coupling of zinc-organic compounds with aryl-halides.[11] This method has been successfully used[12] to prepare 2-aryl-pyridines through the use of *in situ* aryl-zinc compounds generated *via* the reaction of aryl-lithium compounds with $ZnCl_2$. In this study, we successfully demonstrated that dibromo-quinoline **1** can be efficiently arylated in the 2-position using *in situ* ArZnCl and the $Pd(dba)_2/PPh_3$ catalyst, which results in high yields of **5** and **6**. To the best of our knowledge, this is the first example of the utilization of Negishi coupling to prepare 2-aryl-quinolines.

Because the sterically hindered amides and imides of transition metals with *ortho*-substituted aryl fragments usually demonstrate improved performance compared to un-hindered analogues,[6] we selected 2,6-dimethyl- and 2,6-di-isopropyl-anilines for further functionalization of intermediates **2–6** (Scheme 2). The amination of 2-aryl-8-bromoquinolines is fast and selective in the presence of the (*N*-[2′-(dicyclohexylphosphino)[1,1′-biphenyl]-2-yl]-*N*,*N*-dimethylamine) ligand,[13] whereas several attempts to use more accessible phosphines (PPh_3, $P(o\text{-tolyl})_3$, PCy_3) resulted in low yields of the desired compounds.

Preparation of group 4 metal complexes

We found that group 4 complexes based on the new ligand precursors **7–12** can be conveniently generated by their reaction with $ZrBn_4$ or $HfBn_4$ reagents[14] (Scheme 3). This successful synthesis results from the coordination of the metal to the nitrogen atom of the quinoline system with subsequent

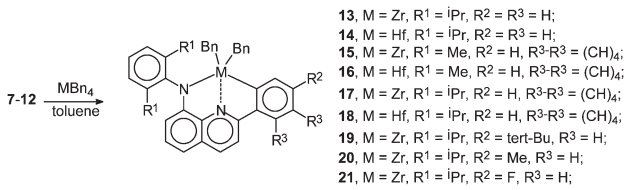

13, M = Zr, R^1 = ^{i}Pr, R^2 = R^3 = H;
14, M = Hf, R^1 = ^{i}Pr, R^2 = R^3 = H;
15, M = Zr, R^1 = Me, R^2 = H, R^3-R^3 = $(CH)_4$;
16, M = Hf, R^1 = Me, R^2 = H, R^3-R^3 = $(CH)_4$;
17, M = Zr, R^1 = ^{i}Pr, R^2 = H, R^3-R^3 = $(CH)_4$;
18, M = Hf, R^1 = ^{i}Pr, R^2 = H, R^3-R^3 = $(CH)_4$;
19, M = Zr, R^1 = ^{i}Pr, R^2 = tert-Bu, R^3 = H;
20, M = Zr, R^1 = ^{i}Pr, R^2 = Me, R^3 = H;
21, M = Zr, R^1 = ^{i}Pr, R^2 = F, R^3 = H;

Scheme 3 Preparation of group 4 metal complexes **13–21**.

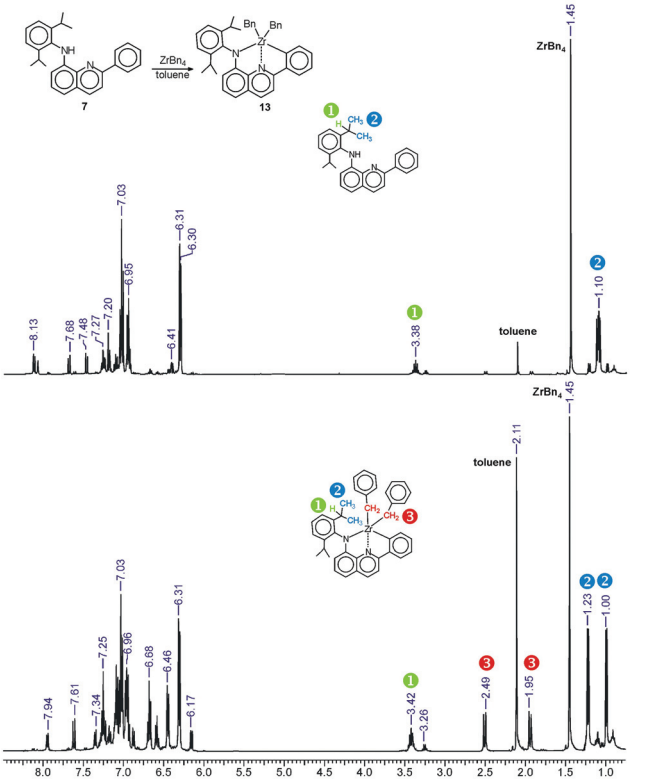

Fig. 2 ^{1}H NMR (400 MHz) monitoring on the reaction of **7** with an excess of $ZrBn_4$ in C_6D_6: after 5 min at 20 °C (top), and after 1 h at 60 °C (bottom).

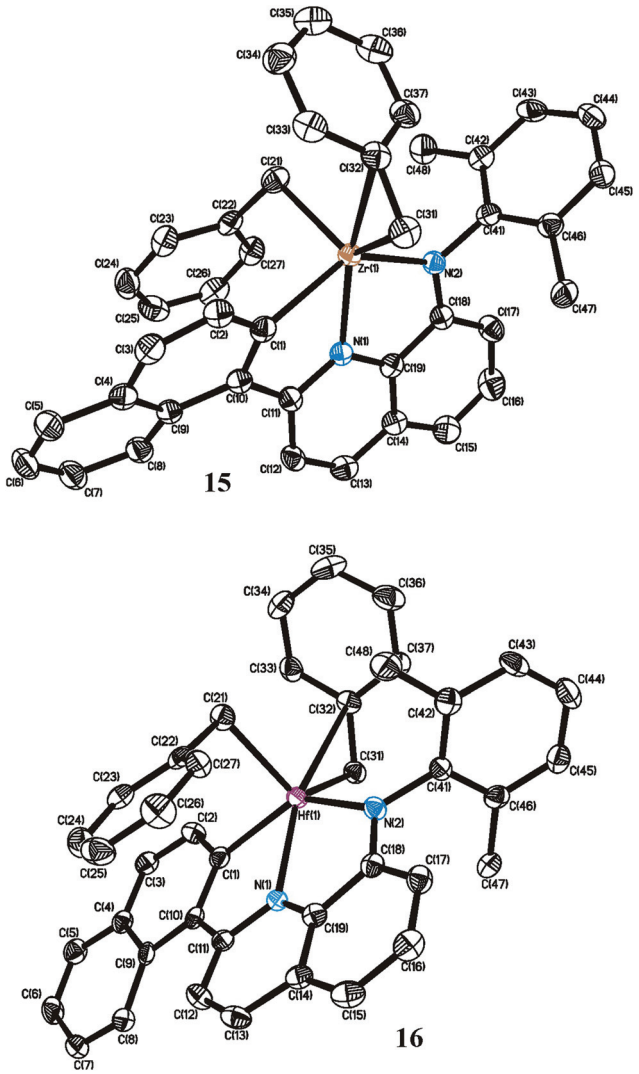

Fig. 3 Molecular structures of **15** and **16**. Displacement ellipsoids are drawn at the 50% probability level. Hydrogen atoms are omitted for clarity.

formation of the intermolecular amide bond and cyclo-metallation through the reaction of the metal center with the 2-aryl group.

Remarkably, the reaction of compounds **7–12** with $ZrBn_4$ is very fast: the combination of the reagents at ambient temperature immediately resulted in the formation of a red solution with a gradual increase in the intensity of the color with time. The reaction is complete in 10–15 h at room temperature, whereas it is complete in approximately 1 h at 60 °C, as confirmed by NMR monitoring of the reaction mixture of compound **7** with an excess of $ZrBn_4$ (Fig. 2).

The reaction is very selective and results in the formation of the sole target complex **13** without the detection of the hypothetical tribenzyl-amide intermediates. The observed high reactivity of the quinoline-based ligand precursors contrasts sharply with the similar reaction of the previously reported pyridine analogues,[15] which usually requires extended heating to complete the process (12–18 h, 70 °C). NMR monitoring of the reaction of the 2,6-diisopropyl-*N*-[[6-(1-naphthyl)-2-pyridinyl](phenyl)-methyl]aniline ligand during the preparation of complex **E** with $ZrBn_4$ also failed to detect the presumable tribenzyl intermediates.[15] The interaction of ligands **7–9** with $HfBn_4$ (Scheme 3) is somewhat slower than with the Zr reagent and requires 4–6 h at 60–70 °C.

The fast and highly selective interaction of quinoline-based [CNN] ligand precursors with the metal source allowed us, in several cases, to circumvent the need to isolate the metal complex pre-catalysts for our polymerization studies and to use the solutions of neutral ligands with the tetra-benzyl metal reagents as *in situ* precursors to prepare the catalysts.

X-ray structure determination of 15, 16, and 18

The structures of closely related dibenzyl Hf and Zr complexes **15**, **16**, and **18** with 2-(8-(phenylamino)quinolin-2-yl)naphthyl-*C*,*N*,*N*′ ligands are shown in Fig. 3 and 4.

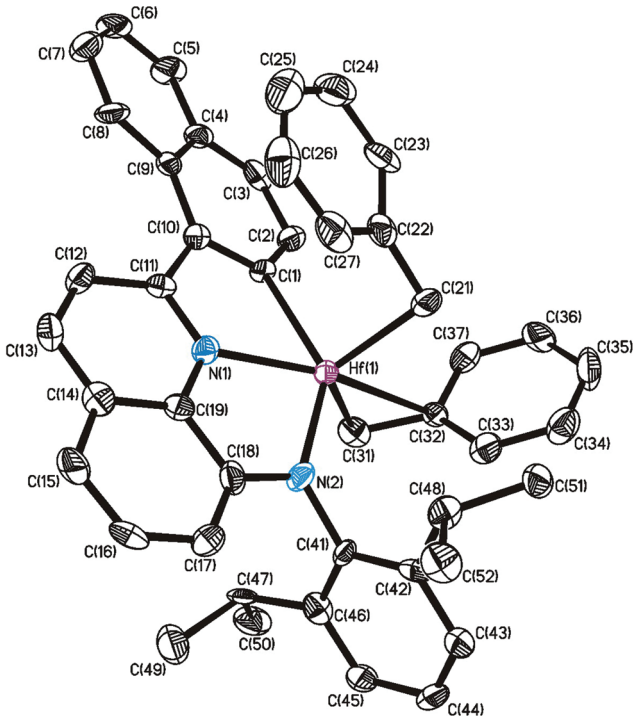

Fig. 4 Molecular structure of **18**. Displacement ellipsoids are drawn at the 50% probability level. Hydrogen atoms are omitted for clarity.

The geometry of the metal core is similar in all three structures. The central metal atoms have irregular coordination polyhedral with CN = 6. Expectedly, the M–N(2) single bonds are approximately 0.15 Å shorter than the M←N(1) coordination bonds.

Both the quinoline and naphthyl moieties are planar within 0.140(6) Å. In all of the structures, these fragments lie in approximately the same plane because the angles between them are 26.7(1), 10.1(1) and 18.2(2)° for **15**, **16**, and **18**, respectively. As a consequence, in all cases, the central metal atoms and the coordinated atoms C(1), N(1), and N(2) also lie in the same planes (within 0.147(3) Å). The C(21) benzyl atoms are arranged approximately perpendicular to these planes, whereas the C(31) benzyl atoms lie in the *trans*-position relative to the N(1) atoms. The M–C(21) and M–C(31) bond lengths are consistent with those expected for Hf and Zr complexes.[16] However, the coordination modes of apical (containing C(21) atoms) and equatorial (containing C(31) atoms) benzyl ligands are noticeably different. All of the M–C(32) distances are significantly shorter than the M–C(22) distances (see Table 1).

On the other side, the C(22)–C(21)–M angles are close to the tetrahedral value, whereas the C(32)–C(31)–M angles (86.0(2)–95.3(5)°) are significantly less than 109.2°.

Thus, the apical benzyl ligand may be treated as η^1-coordinated, whereas the equatorial one represents the η^2-coordination mode. Probably, the latter case is the result of electronic effects induced by the 2-(8-(phenylamino)quinolin-2-yl)naphthyl-ligands. In solution under ambient conditions benzyl groups are equivalent: the signal of $-CH_2$-groups is observed for all complexes as doublet of doublets in ^{1}H NMR spectra with characteristic $^2J \sim 10$–12 Hz (diastereotopic $-CH_2-$ hydrogen atoms), and as a singlet in ^{13}C NMR spectra. No short intermolecular contacts were observed in the structures of **15**, **16**, and **18**. To the best of our knowledge, only two structures of metal complexes (Pt and Pd) bearing 2-aryl-8-quinolinamine ligands have been reported to date.[8b]

Table 1 Selected bond lengths (Å) and angles (°) in **15**, **16**, and **18**

	15, M = Zr	**16**, M = Hf	**18**, M = Hf
M–C(1)	2.295(4)	2.266(3)	2.281(6)
M–N(1)	2.305(3)	2.269(2)	2.274(6)
M–N(2)	2.163(3)	2.128(2)	2.148(6)
M–C(21)	2.285(4)	2.241(3)	2.232(7)
M–C(31)	2.309(4)	2.257(3)	2.234(8)
M–C(22)	3.029(4)	2.894(3)	2.910(8)
M–C(32)	2.646(4)	2.740(3)	2.777(7)
C(22)–C(21)–M	104.9(2)	100.1(2)	101.5(5)
C(32)–C(31)–M	86.0(2)	92.26(19)	95.3(5)

Ethylene/1-butene co-polymerization

A series of ethylene co-polymerization reactions were performed with complexes **13–21**, as well as with the earlier reported C_1-symmetric Hf–pyridylamido complex **E**[6] under industrially relevant slurry polymerization conditions using silica-supported recipes pre-activated with MAO and an optional borate cocatalyst (Table 2).

Under our testing conditions, the Zr complexes were more active than their Hf analogues (complexes **13**, **15**, **17** *vs.* **14**, **16**, **18**, correspondingly). The utilization of a mixed MAO/borate activator results in a further increase in the catalyst productivity compared to the individual components, as illustrated by the comparison of *run 12* to *runs 10* and *11* and further by the comparison of *runs 7 vs. 6* and *24 vs. 23*. The catalyst in this study showed a steep deactivation, as illustrated by the ethylene consumption curves *vs.* time (Fig. 5), which show only a small effect of the polymerization temperature on the profile. The initial, extremely high activity during the first 10 min of the test (50 000 kg mol M^{-1} h^{-1} and higher in some cases) usually decreases to moderate values between 10 000 and 5 000 kg mol M^{-1} h^{-1}. The catalyst samples exhibited a good shelf-life, and, in the case of complex **17**, the catalyst was demonstrated to retain its initial performance in a supported MAO/borate pre-activated recipe for more than 1 month.

The catalysts generated using the new complexes based on the quinoline template show a high molecular weight potential in co-polymerization experiments without H_2; this potential significantly exceeds that of complex **E** based on the pyridine scaffold. The strongly pronounced deactivation kinetic profile of these complexes is a general observation and needs further understanding. Traditional supported metallocenes or magnesium chloride supported Ziegler–Natta catalysts tested in these conditions usually show much less dramatic decay of activity with time.

Table 2 Ethylene co-polymerization with 1-butene with MAO (and optional $[Ph_3C][B(C_6F_5)_4]$)-activated and silica-supported complexes[a]

Run	Complex	Polym. *T*, °C	$[Ph_3C]$ $[B(C_6F_5)_4]$/M molar ratio	H_2, mmol	Activity, kg mol^{-1} M × h	M_w, ×10^3 g mol^{-1}	M_wM_n	Ethyl branches/1000C
1	**E**	70	1.1	0	5491	23.4	15.3	37.8
2	**E**	70	1.1	84.9	2592	Wax		
3	**13**	70	1.1	0	9411	1063	11.7	15.6
4	**13**	70	1.1	84.9	7479	182	8.3	14.6
5	**14**	70	0	0	0			
6	**15**	70	0	0	1033	1594	22.6	15.8
7	**15**	70	1.1	0	5703	Insoluble		20.0
8	**15**	70	1.1	84.9	6794	279	13.4	19.0
9	**16**	70	0	0	0			
10	**17**	70	0	0	1747	1533	16.8	10.2
11[b]	**17**	70	1.1	0	789	1348	97.5	10.3
12	**17**	70	1.1	0	5069	Insoluble		17.4
13	**17**	70	1.1	4.0	9637	804	11.5	16.8
14	**17**	70	1.1	7.9	10 959	507	14.2	16.5
15	**17**	70	1.1	34.0	11 062	476	15.5	14.0
16	**17**	70	1.1	84.9	10 410	287	19.7	17.1
17	**17**	70	1.1	169.8	5735	211	21.2	20.8
18[c]	**17**	70	1.1	169.8	10 624	143	18.0	44.6
19[d]	**17**	70	1.1	169.8	2426	256	42.6	na
20	**17**	55	1.1	169.8	5576	280	24.4	16.6
21	**17**	60	1.1	169.8	7611	266	15.7	18.8
22	**17**	80	1.1	169.8	5660	130	17.5	25.3
23	**18**	70	0	0	0			
24	**18**	70	1.1	0	1068	Insoluble		24.9
25	**19**[e]	70	1.1	0	3811	Insoluble[f]		6.7
26	**19**[e]	70	1.1	84.9	3450	Insoluble[g]		7.2
27	**20**	70	1.1	0	5273	Insoluble		15.0
29	**20**	70	1.1	84.9	4724	255	9.7	13.0
29	**21**	70	1.1	0	6783	Insoluble		18.6
30	**21**	70	1.1	84.9	8908	224	10.5	20.7

[a] Polymerizations were performed in a 2 L autoclave reactor with 3–8 μmol of metal complex in 1 L of isobutene diluent at 15 bar partial pressure of ethylene in the presence of 100 mL of 1-butene co-monomer and 1 mL of 1 M triisobutylaluminum scavenger. The supported catalyst was injected into an equilibrated reactor at the polymerization temperature and pressure, and the ethylene pressure was maintained throughout the 30–60 min test. The silica-supported catalysts were prepared by dissolving the optional $[Ph_3C][B(C_6F_5)_4]$ cocatalyst in 4.21 M MAO solution in toluene, followed by the complex (Al : B : metal: 200 : 1.1 : 1) and adding the resulting solution to a silica support calcined at 600 °C; this reaction resulted in a free-flowing powder, which was aged overnight before testing. [b] The $[Ph_3C]$-$[B(C_6F_5)_4]$ was used only as an activator. [c] A short, 11 min run. [d] Homopolymerization of ethylene. [e] Complex prepared *in situ* by reacting an equimolar amount of complex **19** with tetrabenzylzirconium. [f] The intrinsic viscosity determined in decalin at 145 °C was 18.2 dl g^{-1}. [g] The intrinsic viscosity determined in decalin at 145 °C was 17.7 dl g^{-1}.

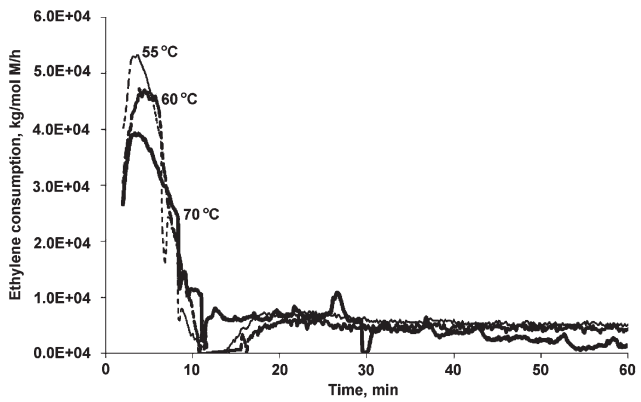

Fig. 5 Ethylene consumption curves in runs **20** (55 °C), **21** (60 °C) and **17** (70 °C) in co-polymerization tests conducted in the presence of 169.8 mmol of H_2 with a catalyst based on complex **17**.

When the samples were sufficiently soluble to allow gel permeation chromatography (GPC), the M_w was greater than 10^6 g mol^{-1}. Hydrogen is an effective chain-transfer agent in the polymerization that allows the molecular weight to be controlled over a broad range of values (Fig. 6, Table 2). All polymers produced with the new catalyst exhibit a broad molecular-weight distribution (Table 2), which indicates the presence of several active sites.

Although various sites generated from the same precursor are likely to already be present in the pre-activated supported catalyst before the test, the transformation of the existing sites is clearly indicated to continue during the polymerization, as illustrated by the effect of residence time in *runs 17* and *18* on the M_w, M_w/M_n and GPC profiles (Table 2, Fig. 7). The co-monomer incorporation level in the ethylene–butene

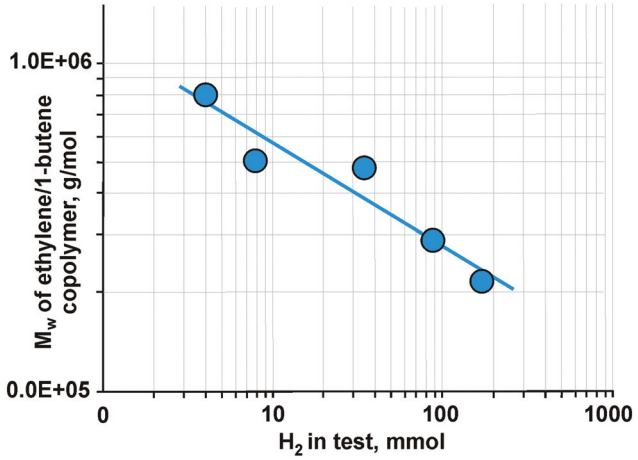

Fig. 6 Effect of H_2 on the M_w of ethylene/1-butene copolymer from polymerization tests at 70 °C and 15 bar ethylene partial pressure using a catalyst based on complex **17**.

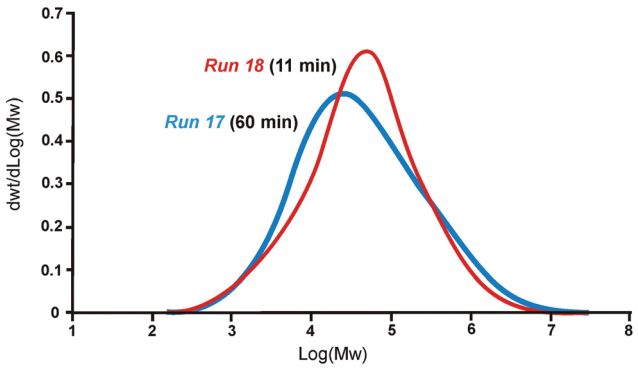

Fig. 7 GPC profiles of polymers prepared with a catalyst based on complex **17** with different residence time in the reactor: 11 min in *run 18* (red line) and 1 h in *run 17* (blue line).

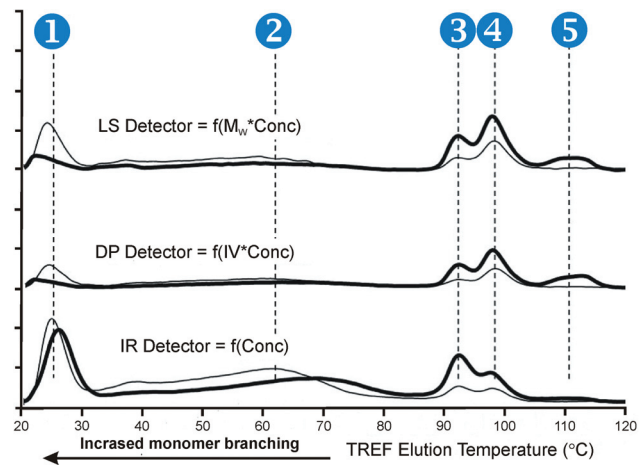

Fig. 8 3D-TREF profiles of ethylene–butene copolymer samples prepared with complex **17** using short (thin line) and long (bold line) residence times.

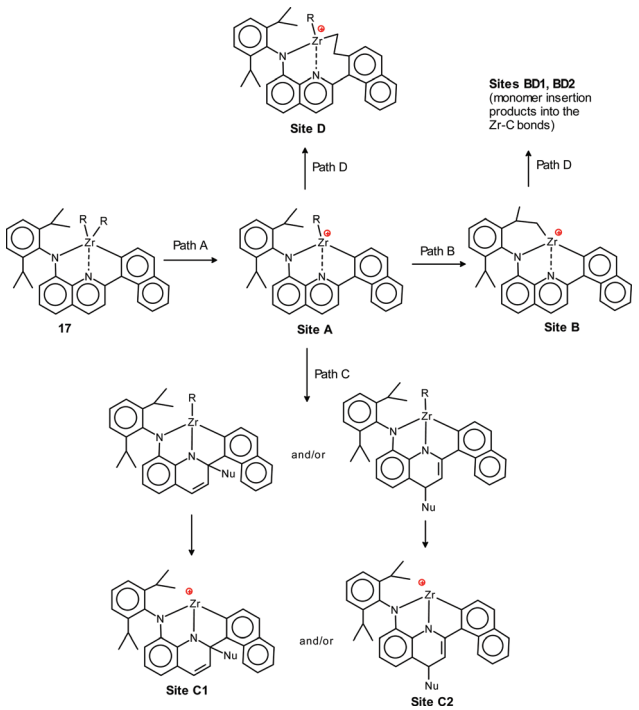

Scheme 4 Site diversification for quinoline-based complexes: the more obvious processes.

copolymer samples also changes with residence time, with the sample prepared in 11 min showing twice the average number of ethyl branches compared to the 1 h sample. This result implies that the balance of sites shifts with time toward those with higher M_w potentials and reduced co-monomer incorporation ability.

This conclusion is confirmed by the 3D-TREF analysis of the samples from *runs 17* and *18* (Fig. 8), which shows at least five polymer modes with various degrees of branching from the highest (1) to the lowest (5). The relative contribution of the less-branched modes (3)–(5) clearly increases with residence time relative to the contribution of the highly branched fractions (1) and (2).

A comparison of the intensities of the peaks detected by the infra-red detector (a measure of polymer concentration) *vs.* the light scattering and viscosity detectors (a combined measure of both concentration and M_w) indicates that the less-branched modes have a higher molecular weight, whereas the highly branched modes have low molecular weights. This difference in molecular weights results in a branching distribution in the samples that is similar to that observed with Ti-based Ziegler–Natta catalysts.[18]

Site diversification processes

Metallocene-based polymerization catalysts are usually single-site systems, the ancillary cyclopentadienyl-type ligands are not involved in specific interactions with the cocatalyst and polymerization medium, resulting in a Flory-like molecular weight distribution. This situation is frequently not the case with "post-metallocene" catalyst precursors based on chelating

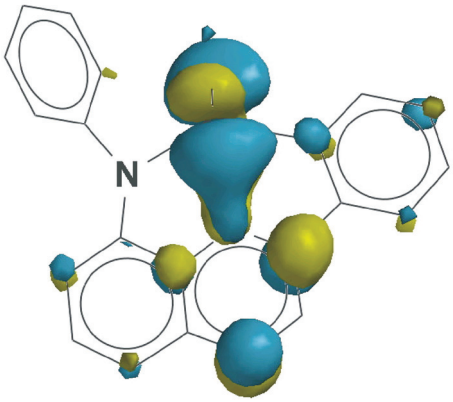

Fig. 9 Localization of the lowest unoccupied orbital in the cationic site Type A (Scheme 4) calculated using the hybrid DFT method B3LYP/6-31G** (Spartan '06, Wavefunction, Inc.).

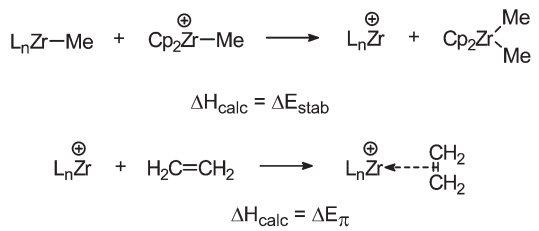

Scheme 5 Model reactions used to define the reactivity indexes.

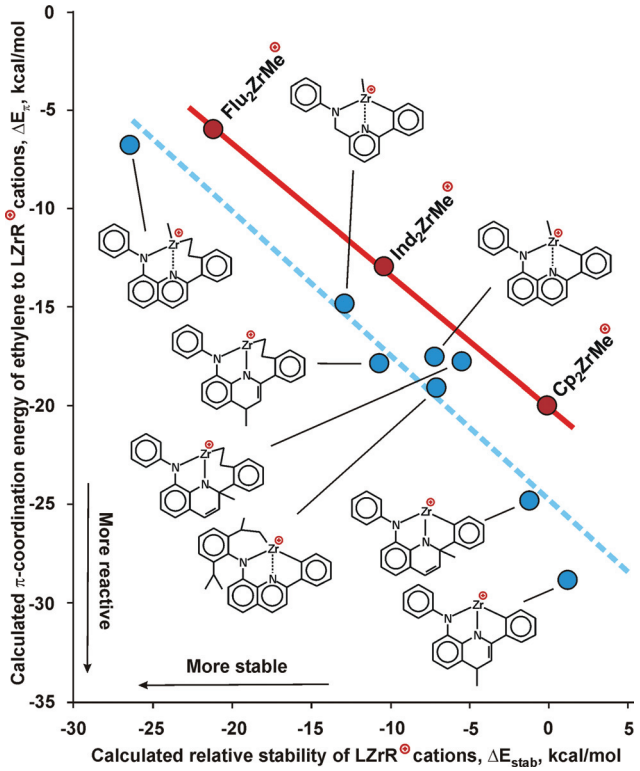

Fig. 10 Relative stabilization (ΔE_{stab}) of hypothetic cationic active site models *vs.* their ethylene coordination energy (ΔE_{π}) calculated using the hybrid DFT method B3LYP/6-31G** (Spartan '06, Wavefunction, Inc.).

ligands. The literature contains numerous indications of site diversification during complex activation[17] and in the process of polymerization.[15] This site diversification is the case for the new quinoline-based complexes, as indicated by the analysis of the microstructure of polymerization products discussed in the previous section. Scheme 4 summarizes the more obvious processes that lead to a large variety of hypothetical active sites.

The obvious primary Sites A, which are generated *via* the usual path of leaving-group abstraction and alkylation by a cocatalyst (Path A, Scheme 4), are expected to undergo secondary transformation during activation or ageing (Paths B and C) and during the polymerization process. Path B involves metallation of the substituent in the amido-phenyl ring, as was demonstrated in a recent paper,[15] whereas Path C is initiated by a nucleophilic attack (*e.g.*, Me– from the MAO activator) at the quinoline ring at positions with high LUMO orbital coefficients (Fig. 9).

The resulting Sites C (Scheme 4) can initiate the polymerization process *via* insertion into the Zr–C_{Ar} bond and can continue the polymerization at the centers stabilized by the resulting bidentate [N–N] ligand. The site diversification along Path D during the polymerization process is similar to the process proposed earlier for the related pyridylamido systems.[17]

Due to very high activity of these new catalysts used in very small quantities in our testing conditions, *in situ* or post-reaction monitoring of the nature and transformation of active components using analytical techniques is unrealistic. While we are considering a future continuation of this study of using model homogeneous systems and polymerization conditions, we turned to computational estimates to rationalize our observations.

To estimate the effect of site diversification on the properties of the resulting hypothetical active species, the geometry of various methylated precursors and the corresponding cations and π-complexes with ethylene were optimized using the hybrid DFT method B3LYP/6-31G[19] implemented in the Spartan '06 package. The resulting energies were used to determine the reactivity indexes ΔE_{stab} (relative stability) and ΔE_{π} (reactivity toward ethylene) based on the calculated enthalpies of the model reactions in Scheme 5. While the exact nature of rate limiting steps in the polymerization process based on these catalysts is not clear (site activation, monomer coordination or insertion, *etc.*), we thought that these very simple indexes provide a fair ranking of stability/reactivity of the hypothetical sites. The calculated energies of the fully optimized structures and atomic coordinates of the cationic models are provided in the ESI.†

The resulting values, as plotted in the chart in Fig. 10, indicate a broad range of variation of the expected properties of the active species proposed in Scheme 4. This range exceeds that observed for the series of metallocenes-type analogues. The trends indicated in Fig. 10 show a stronger π-coordination

ability of the chelate-complexes compared to that of the metallocenes at the same level of active-site stabilization.

Conclusions

The diversity of possible ligand environments and the vastness of experimentally "uncharted territories" ensure a promising and vibrant future for the development of new catalysts for enhanced products at reduced manufacturing costs. An integrated catalyst–process–product design strategy should be based on convenient synthesis strategies of ligand candidates starting from easily accessible precursors and inexpensive procedures. This study capitalizes on such an approach by taking advantage of the uniquely diverse topologies offered by the quinoline scaffold combined with convenient synthetic coupling procedures.

Although the replacement of the stabilizing ancillary cyclopentadienyl ligands of the traditional metallocenes with the chelating ligands in the post-metallocene systems of recent years led to a broad diversity of new catalysts and generated new polyolefins with unique microstructures, it also resulted, in many cases, in the loss of the comforting "simplicity" of the single-site paradigm. The higher inherent reactivity of the new ligands compared to that of the cyclopentadienyl analogues toward the components of catalyst recipes usually leads to the generation of multiple active sites and a stronger sensitivity of the polymer microstructure to the composition of the catalyst and process conditions, as is clearly demonstrated in this contribution. The more complicated microstructure of these new polymers compared to the materials with narrow polydispersity prepared with true single-site catalysts could result in unique and beneficial balance of performance attributes, such as an improved processability of the produced polymers combined with a higher molecular-weight potential.

Experimental

Materials and methods

All operations with group IV metal benzyl derivatives were performed under argon using standard Schlenk technique or under vacuum using a sealed glass "equipped-with-everything" system. Phenylboronic acid,[20] 1-naphthylboronic acid,[21] 4-*tert*-butylphenylboronic acid,[22] 2,8-dibromoquinoline,[8] tri(*o*-tolyl)-phosphine,[23] $Pd(dba)_2$,[24] and *N*-[2′-(dicyclohexylphosphino)-[1,1′-biphenyl]-2-yl]-*N*,*N*-dimethylamine[25] were prepared in accordance with published procedures. Samples of group IV metal benzyl derivatives were prepared by condensation of dried (over Na/benzophenone/dibenzo-18-crown-6) and degassed deuterated solvents (C_6D_6 or toluene-d_8) into NMR tubes containing 5–10 mg of the complexes.

Preparation of Zr and Hf complexes

Dibenzylzirconium *N*-(2,6-diisopropylphenyl)-2-phenyl-8-quinolinamide (13). A solution of tetrabenzylzirconium (1.56 g, 3.42 mmol) in toluene–hexane (3 : 2, 25 mL) was added at 0 °C to a solution of **7** (1.09 g, 2.85 mmol) in toluene–hexane (3 : 2, 25 mL). The mixture was allowed to warm to room temperature (the color of the mixture changed from pale-yellow to red within several minutes), stirred for 6 h at 50–60 °C, and evaporated. The residue was recrystallized from hexane. The yield was 0.95 g (51%). $C_{41}H_{40}N_2Zr$ (652.00): calcd C 75.53, H 6.18, N, 4.30; found C 75.50, H 6.22, N 4.33. ^{1}H NMR (400 MHz, C_6D_6, 20 °C) δ: 7.97 (d, 1H, ^3J = 7.0 Hz), 7.62 (d, 1H, ^3J = 8.6 Hz), 7.35 (d, 1H, ^3J = 7.7 Hz), 7.27–6.86 (groups of m, 8H, aromatic H), 6.68 (t, 4H, ^3J = 7.5 Hz), 6.58 (t, 2H, ^3J = 7.5 Hz), 6.45 (d, 4H, ^3J = 7.5 Hz, $-CH_2C_6H_5$), 6.16 (d, 1H, ^3J = 7.7 Hz, Zr–C≡C–*H*), 3.42 (sept, 2H, ^3J = 6.8 Hz, $-CH(CH_3)_2$), 2.50 (d, 2H, ^2J = 10.4 Hz, $-CH_2C_6H_5$), 1.94 (d, 2H, ^2J = 10.4 Hz, $-CH_2C_6H_5$), 1.22 (d, 6H, ^3J = 6.8 Hz, $-CH(CH_3)_2$), 1.00 (d, 6H, ^3J = 6.8 Hz, $-CH(CH_3)_2$).

Dibenzylhafnium *N*-(2,6-diisopropylphenyl)-2-phenyl-8-quinolinamide (14). A solution of tetrabenzylhafnium (0.71 g, 1.3 mmol) in toluene (10 mL) was added at 0 °C to a solution of **7** (0.38 g, 1 mmol) in toluene (10 mL). The color of the mixture changed from pale-yellow to dark red. The resulting mixture was allowed to warm to room temperature and was then stirred for 8 h at 60–70 °C. The mixture was evaporated, and hexane (20 mL) was added. The crystalline precipitate was separated by decantation, washed by pentane and dried *in vacuo*. The product was a red crystalline powder with a yield of 0.36 g (48%). $C_{41}H_{40}HfN_2$ (739.27): calcd C 66.61, H 5.45, N 3.79; found C 66.55, H 5.55, N 3.82. ^{1}H NMR (400 MHz, C_6D_6, 20 °C) δ: 8.26 (d, 1H, ^3J = 7.2 Hz), 7.53 (d, 1H, ^3J = 8.8 Hz), 7.43 (d, 1H, ^3J = 7.7 Hz), 7.38 (t, 1H, ^3J = 7.3 Hz), 7.35–7.01 (groups of m, 6H), 6.81 (d, 1H, ^3J = 7.3 Hz, aromatic H), 6.75 (t, 4H, ^3J = 7.4 Hz), 6.62 (m, 6H, $-CH_2C_6H_5$), 6.21 (d, 1H, ^3J = 7.7 Hz, Hf–C≡C–*H*), 3.55 (sept, 2H, ^3J = 6.9 Hz, $-CH(CH_3)_2$), 2.46 (d, 2H, ^2J = 11.9 Hz, $-CH_2C_6H_5$), 2.16 (d, 2H, ^2J = 11.9 Hz, $-CH_2C_6H_5$), 1.26 (d, 6H, ^3J = 6.9 Hz, $-CH(CH_3)_2$), 1.03 (d, 6H, ^3J = 6.9 Hz, $-CH(CH_3)_2$).

Dibenzylzirconium *N*-(2,6-dimethylphenyl)-2-(1-naphthyl)-8-quinolinamide (15). A solution of tetrabenzylzirconium (1.10 g, 2.4 mmol) in toluene (10 mL) was added at 0 °C to a solution of **8** (0.75 g, 2 mmol) in toluene (20 mL). The color of the mixture changed from pale-yellow to dark red. The resulting mixture was allowed to warm to room temperature and was then stirred for 4 h at 50 °C. The mixture was concentrated to approximately 10 mL, and hexane (20 mL) was added. The crystalline precipitate was separated by decantation, washed with pentane and dried *in vacuo*. The product was a red-violet crystalline powder, and the yield was 0.74 g (57%). $C_{41}H_{34}N_2Zr$ (645.95): calcd C 76.24, H 5.31, N 4.34; found C 76.12, H 5.39, N 4.35. ^{1}H NMR (400 MHz, toluene-d_8, 20 °C) δ: 8.38 (d, 1H, ^3J = 8.4 Hz), 8.06 (d, 1H, ^3J = 7.9 Hz), 7.97 (d, 1H, ^3J = 8.8 Hz), 7.69 (t, 2H, ^3J = 8.8 Hz), 7.54 (d, 1H, ^3J = 7.9 Hz), 7.40–7.27 (m, 4H), 7.17–6.96 (m, 3H, aromatic H), 6.60 (t, 4H, ^3J = 7.5 Hz), 6.53 (t, 2H, ^3J = 7.5 Hz), 6.39 (d, 4H, ^3J = 7.5 Hz, $-CH_2C_6H_5$), 6.18 (d, 1H, ^3J = 7.5 Hz, Zr–C≡C–*H*), 2.30 (d, 2H, ^2J = 10.1 Hz, $-CH_2C_6H_5$), 2.16 (s, 3H, $-CH_3$), 2.11 (s, 3H, $-CH_3$), 1.81 (d, 2H, ^2J = 10.1 Hz, $-CH_2C_6H_5$).

Dibenzylhafnium *N*-(2,6-dimethylphenyl)-2-(1-naphthyl)-8-quinolinamide (16). The synthesis of **16** was carried out in the same way as that described for **15**, but tetrabenzylhafnium was used, and the reaction time was 8 h at 60–70 °C. The yield was 63%. $C_{41}H_{34}HfN_2$ (733.22): calcd C 67.16, H 4.67, N 3.82; found C 67.12, H 4.70, N 3.85. ^{1}H NMR (400 MHz, toluene-d_8, 20 °C) δ: 8.34 (d, 1H, ^3J = 8.5 Hz), 8.18 (d, 1H, ^3J = 8.0 Hz), 7.97 (d, 1H, ^3J = 8.7 Hz), 7.58 (t, 2H, ^3J = 8.7 Hz), 7.45–7.15 (m, 5H), 7.05–6.70 (m, 3H), 6.50–6.30 (m, 10H, aromatic H), 6.09 (d, 1H, ^3J = 7.7 Hz, Hf–C=C–*H*), 2.28 (d, 2H, ^2J = 10.5 Hz, –C*H*$_2$C$_6$H$_5$), 2.22 (s, 3H, –CH$_3$), 2.15 (s, 3H, –CH$_3$), 1.98 (d, 2H, ^2J = 10.5 Hz, –C*H*$_2$C$_6$H$_5$).

Dibenzylzirconium *N*-(2,6-diisopropylphenyl)-2-(1-naphthyl)-8-quinolinamide (17). A solution of tetrabenzylzirconium (1.23 g, 2.7 mmol) in toluene (10 mL) was added at 0 °C to a solution of **9** (0.95 g, 2.2 mmol) in toluene (20 mL). The color of the mixture changed from pale-yellow to dark-red. The resulting mixture was allowed to warm to room temperature and then stirred for 8 h at 60 °C. The toluene was evaporated, and the residue was extracted with pentane. The product crystallizes slowly! The product was a red–violet powder, and the yield was 0.55 g (36%). $C_{45}H_{42}N_2Zr$ (702.06): calcd C 76.99, H 6.03, N 3.99; found C 76.88, H 6.11, N 4.08. ^{1}H NMR (400 MHz, C_6D_6, 20 °C) δ: 8.35 (d, 1H, ^3J = 8.3 Hz), 8.15 (d, 1H, ^3J = 7.8 Hz), 7.94 (d, 1H, ^3J = 8.9 Hz), 7.72 (m, 2H), 7.66 (d, 1H, ^3J = 8.7 Hz), 7.60 (d, 1H, ^3J = 7.7 Hz), 7.39–7.06 (m, 4H, aromatic H), 6.67 (t, 4H, ^3J = 7.4 Hz), 6.58 (m, 6H, –CH$_2$C$_6$*H*$_5$), 6.30 (d, 1H, ^3J = 8.5 Hz, Zr–C=C–*H*), 3.52 (sept, 2H, ^3J = 6.8 Hz, –C*H*(CH$_3$)$_2$), 2.57 (d, 2H, ^2J = 10.3 Hz, –C*H*$_2$C$_6$H$_5$), 2.10 (d, 2H, ^2J = 10.3 Hz, –C*H*$_2$C$_6$H$_5$), 1.26 (d, 6H, ^3J = 6.8 Hz, –CH(C*H*$_3$)$_2$), 1.05 (d, 6H, ^3J = 6.8 Hz, –CH(C*H*$_3$)$_2$).

Dibenzylhafnium *N*-(2,6-diisopropylphenyl)-2-(1-naphthyl)-8-quinolinamide (18). The synthesis of **18** was carried out in the same way as that described for **15**, but tetrabenzylhafnium and ligand **9** were used, and the reaction time was 8 h at 60 °C. The product was a red crystalline powder, and the yield was 54%. $C_{45}H_{42}HfN_2$ (789.33): calcd C 68.47, H 5.36, N 3.55; found C 68.50, H 5.44, N 3.50. ^{1}H NMR (400 MHz, C_6D_6, 20 °C) δ: 8.41 (d, 1H, ^3J = 7.7 Hz), 8.31 (d, 1H, ^3J = 8.2 Hz), 7.89 (d, 1H, ^3J = 8.8 Hz), 7.76 (d, 1H, ^3J = 7.7 Hz), 7.73 (d, 1H, ^3J = 7.7 Hz), 7.57 (m, 2H, ^3J = 8.8 Hz), 7.40–7.11 (m, 4H), 6.85 (d, 1H, ^3J = 8.1 Hz, aromatic H), 6.69 (t, 4H, ^3J = 7.5 Hz), 6.65 (d, 4 H, ^3J = 7.5 Hz), 6.57 (t, 2H, ^3J = 7.5 Hz, –CH$_2$C$_6$*H*$_5$), 6.27 (d, 2H, ^3J = 7.7 Hz, Hf–C=C–*H*), 3.59 (sept, 2H, ^3J = 6.8 Hz, –C*H*(CH$_3$)$_2$), 2.45 (d, 2H, ^2J = 11.9 Hz, –C*H*$_2$C$_6$H$_5$), 2.22 (d, 2H, ^2J = 11.9 Hz, –C*H*$_2$C$_6$H$_5$), 1.28 (d, 6H, ^3J = 6.8 Hz, –CH(C*H*$_3$)$_2$), 1.06 (d, 6H, ^3J = 6.8 Hz, –CH(C*H*$_3$)$_2$). ^{13}C NMR (100 MHz, C_6D_6, 20 °C) δ: 154.3, 146.8, 143.1, 141.4, 141.0, 139.7, 132.5, 129.8, 129.3, 128.8, 128.5, 127.6, 127.5, 126.9, 125.4, 125.2, 124.5, 123.7, 121.3, 114.1, 113.3, 83.5, 28.8, 27.1, 23.6.

Dibenzylzirconium *N*-(2,6-diisopropylphenyl)-2-(4-*tert*-butylphenyl)-8-quinolinamide (19). A solution of tetrabenzylzirconium (1.86 g, 4.08 mmol) in hexane–toluene (3 : 2, 30 mL) was added at 0 °C to a solution of **10** (1.48 g, 3.4 mmol) in hexane–toluene (3 : 2, 30 mL). The mixture was allowed to warm to room temperature and was then stirred for 6 h at 50–60 °C and evaporated. The residue was recrystallized from hexane (30 mL). The precipitate (side product) was filtered off, and the mother liquor was evaporated and dried to yield a red–violet glass solid. The yield was 1.52 g (63%). $C_{45}H_{48}N_2Zr$ (708.10): calcd C 76.33, H 6.83, N 3.96; found C 76.30, H 6.95, N 4.04. ^{1}H NMR (400 MHz, C_6D_6, 20 °C) δ: 8.10 (bs, 1H), 7.64 (d, 2H, ^3J = 8.6 Hz), 7.41–6.93 (group of m, 6H), 6.79 (t, 4H, ^3J = 7.7 Hz), 6.65 (t, 2H, ^3J = 7.7 Hz), 6.60 (d, 4H, ^3J = 7.7 Hz), 6.39 (d, 2H, ^3J = 7.3 Hz, aromatic H), 6.25 (d, 1H, ^3J = 7.7 Hz, Zr–C=C–*H*), 3.51 (sept, 2H, ^3J = 6.8 Hz, –C*H*(CH$_3$)$_2$), 2.66 (d, 2H, ^2J = 10.3 Hz, –C*H*$_2$C$_6$H$_5$), 1.98 (d, 2H, ^2J = 10.3 Hz, –C*H*$_2$C$_6$H$_5$), 1.40 (s, 9H, –C(CH$_3$)$_3$), 1.27 (d, 6H, ^3J = 6.8 Hz, –CH(C*H*$_3$)$_2$), 1.04 (d, 6H, ^3J = 6.8 Hz, –CH(C*H*$_3$)$_2$).

Dibenzylzirconium *N*-(2,6-diisopropylphenyl)-2-(4-methylphenyl)-8-quinolinamide (20). A solution of tetrabenzylzirconium (1.25 g, 2.74 mmol) in hexane–toluene (1 : 1, 20 mL) was added at 0 °C to a solution of **11** (0.90 g, 2.28 mmol) in hexane–toluene 1 : 1 (20 mL). The mixture was allowed to warm to room temperature and was then stirred for 6 h at 50–60 °C. The color of the mixture changed from pale-yellow to dark-red. The mixture was concentrated to 10 mL, hexane (30 mL) was added, and the red–violet precipitate of by-product was separated by decantation. The mother liquor was then evaporated, and the residue was recrystallized from pentane to yield 0.44 g (29%) of the product (dark-red crystalline powder). $C_{42}H_{42}N_2Zr$ (666.02): calcd C 75.74, H 6.36, N 4.21; found C 75.70, H 6.46, N 4.10. ^{1}H NMR (400 MHz, C_6D_6, 20 °C) δ: 7.60 (d, 1H, ^3J = 8.6 Hz), 7.38 (d, 1H, ^3J = 7.7 Hz), 7.30–6.95 (groups of m, 6H), 6.91 (d, 1H, ^3J = 8.8 Hz, aromatic H), 6.76 (t, 4H, ^3J = 7.7 Hz), 6.60 (m, 6H, –CH$_2$C$_6$*H*$_5$), 6.39 (d, 1H, ^3J = 7.0 Hz), 6.20 (d, 1H, ^3J = 7.8 Hz, Zr–C=C–*H*), 3.49 (sept, 2H, ^3J = 6.8 Hz, –C*H*(CH$_3$)$_2$), 2.64 (d, 2H, ^2J = 10.4 Hz, –C*H*$_2$C$_6$H$_5$), 2.31 (s, 3H, –CH$_3$), 2.12 (d, 2H, ^2J = 10.4 Hz, –C*H*$_2$C$_6$H$_5$), 1.25 (d, 6H, ^3J = 6.8 Hz, –CH(C*H*$_3$)$_2$), 1.02 (d, 6H, ^3J = 6.8 Hz, –CH(C*H*$_3$)$_2$).

Dibenzylzirconium *N*-(2,6-diisopropylphenyl)-2-(4-fluorophenyl)-8-quinolinamide (21). A solution of tetrabenzylzirconium (1.34 g, 2.95 mmol) in hexane–toluene (1 : 1, 20 mL) was added at 0 °C to a solution of **12** (0.98 g, 2.46 mmol) in hexane–toluene (1 : 1, 20 mL). The mixture was allowed to warm to room temperature and was then stirred for 6 h at 50–60 °C. The color of the mixture changed from pale-yellow to red–violet, and a precipitate formed. The volume of the mixture was reduced to 10 mL, hexane (30 mL) was added, and the red–violet precipitate of by-product was separated by decantation. The mother liquor was then evaporated, and the residue was recrystallized from pure hexane to yield 0.37 g (22%) of the product (dark-red crystalline powder). $C_{41}H_{39}FN_2Zr$ (669.99): calcd C 73.50, H 5.87, N 4.18; found C 73.59, H 5.99, N 4.10. ^{1}H NMR (400 MHz, C_6D_6, 20 °C) δ: 7.73 (dd, 1H, ^3J = 7.7 Hz, $^3J_{H-F}$ = 2.8 Hz), 7.60 (d, 1H, ^3J = 8.6 Hz), 7.29–6.37 (groups of m, 18H, aromatic H), 6.20 (d, 1H, ^3J = 8.6 Hz, Zr–C=C–*H*), 3.44 (sept, 2H, ^3J = 6.6 Hz, –C*H*(CH$_3$)$_2$), 2.56 (d, 2H, ^2J = 10.3 Hz, –C*H*$_2$C$_6$H$_5$), 1.90 (d, 2H, ^2J = 10.3 Hz, –C*H*$_2$C$_6$H$_5$), 1.22 (d, 6H, ^3J = 6.6 Hz, –CH(C*H*$_3$)$_2$), 1.00 (d, 6H, ^3J = 6.6 Hz, –CH(C*H*$_3$)$_2$).

Table 3 Crystal data, data collection and refinement parameters for **15**, **16**, and **18**

	15	16	18
Formula	$C_{41}H_{34}Zr_1N_2$	$C_{41}H_{34}Hf_1N_2$	$C_{51}H_{48}Hf_1N_2$
Formula weight	645.92	733.19	867.40
Colour, habit	Block, black	Prism, pink	Red, plate
Cryst size, mm	0.25 × 0.20 × 0.15	0.08 × 0.08 × 0.03	0.15 × 0.06 × 0.01
Cryst syst	Monoclinic	Monoclinic	Monoclinic
Space group	$P2_1/c$	$P2_1/c$	$P2_1/c$
a, Å	14.660(3)	8.0530(5)	13.693(4)
b, Å	13.776(2)	19.1170(11)	16.488(5)
c, Å	16.926(3)	20.0917(12)	17.561(6)
β, °	114.325(2)	101.416(1)	99.135(6)
V, Å^3	3114.8(10)	3031.9(3)	3915(2)
Z	4	4	4
d_{calc}, g cm^{-3}	1.377	1.606	1.472
μ, mm^{-1}	0.385	3.474	2.703
F(000)	1336	1464	1760
θ range, °	1.52 to 26.00	1.48 to 27.00	1.70 to 25.25
Total no. of reflns	22 834	23 800	28 148
Unique reflns	6061	6616	7050
R_{int}	0.0476	0.0394	0.1383
No. with $I > 2\sigma(I)$	4729	4957	4539
No. of variables	399	399	492
R_1 ($I > 2\sigma(I)$)	0.0495	0.0262	0.0510
wR_2 (all data)	0.1426	0.0571	0.1033
GOOF on F^2	1.079	1.018	0.923
Largest diff peak/hole, e Å^{-3}	0.941/−0.686	0.775/−0.516	1.240/−1.108

X-ray structural determinations of 15, 16, and 18

Experimental intensities were measured on a Bruker SMART APEX II diffractometer using graphite-monochromated Mo-$K\alpha$ radiation (λ = 0.71073 Å) at 150 K. Absorption corrections based on measurements of equivalent reflections were applied.[26] The structures were solved by direct methods and were refined by a full-matrix least-squares on F^2 [27] with anisotropic thermal parameters for all non-hydrogen atoms. In all structures, all hydrogen atoms were placed in calculated positions and refined using a riding model. Details of the X-ray investigations are given in Table 3.

General procedure for the preparation of supported catalyst samples

Trityl tetrakis(pentafluorophenyl)borate (0.052 g, 0.56 mmol) was added to 2.2 mL of a 4.21 M solution of MAO in toluene (Albemarle) and stirred for 15 min. A specified amount of complex precursor (to achieve an Al–metal molar ratio of 200) was added to the resulting solution, which was stirred for an additional 15 min. The resulting homogeneous solution was slowly and evenly added to a stirred bed of 2 g of silica support (Davison C948, calcined for 6 h at 600 °C), which resulted in a free-flowing catalyst powder, which was used in polymerization tests after being aged at least overnight.

General procedure for polymerization tests

A jacketed 2 L stainless steel stirred autoclave was charged with 1 L of isobutane diluent, triisobutylaluminum scavenger (1 mL of a 1 M solution in hexanes), 100 mL of 1-butene co-monomer and, optionally, hydrogen. The contents were heated to the desired polymerization temperature and pressurized with 15 bar of ethylene partial pressure. After the mixture was allowed to equilibrate for 15 min, the polymerization was initiated by the injection of the catalyst powder with a small amount of isobutane. The temperature and pressure was maintained throughout the run by supplying ethylene on-demand. The polymerization was usually terminated after 1 h by cooling and venting the volatile contents of the reactor.

Polymer analysis

Molecular weight and molecular weight distributions were determined by GPC (gel permeation chromatography). Measurements were conducted on a Waters GPCV-LS 2000 with three Polymer Lab Olexis columns. The solvent was trichlorobenzene (TCB), and the temperature was 145 °C. Selected GPC traces of products are provided in the ESI.† The flow rate was 1.0 mL min^{-1}. TREF (temperature rising elution fractionation) was used to characterize the co-monomer distribution of the polymers. In a TREF measurement, the sample is first dissolved in a solvent (ODCB) at an elevated temperature (150 °C); the solution is then cooled slowly so that the polymer crystallizes in layers around small beads in a chromatographic column based on differences in solubility (crystallizability) of various polymer fractions; in the elution step, the solvent is heated at a controlled rate, and the concentration of the polymer dissolved in the solvent is continuously monitored. Triple detectors in 3D-TREF allow for the continuous monitoring of concentration (IR detector), solution viscosity (viscometer), and molecular weight (light-scattering detector) of the eluting fractions. Fractions with a high level of co-monomer branching are more soluble and elute at lower temperatures than fractions with lower levels of co-monomer branching. The viscometer and light-scattering signals provide an indication of the relative molecular weights of the various fractions. Details of the 3D-TREF technique are described elsewhere.[28]

Acknowledgements

We thank LyondellBasell Industries for financial support and for permission to publish this work.

Notes and references

1 V. C. Gibson and S. K. Spitzmesser, *Chem. Rev.*, 2003, **103**, 283, and references therein.
2 (*a*) H. Makio, N. Kashiwa and T. Fujita, *Adv. Synth. Catal.*, 2002, **344**, 477; (*b*) H. Makio, H. Terao, A. Iwashita and T. Fujita, *Chem. Rev.*, 2011, **111**, 2363, and references therein.
3 V. C. Gibson, C. Redshaw and G. A. Solan, *Chem. Rev.*, 2007, **107**, 1745, and references therein.

4 (*a*) E. Y. Tshuva, I. Goldberg and M. Kol, *J. Am. Chem. Soc.*, 2000, **122**, 10706; (*b*) M. Kol and E. Tshuva (Univ. Lamot), Appl. US6686490, 2004.
5 A. M. Johns (Univation Tech LLC), Appl. WO2010053696, 1999.
6 (*a*) A. Vogel and E. M. Carnahan (DOW Global Technologies, Inc.), Appl. WO2004024740, 2004; (*b*) A. Vogel (DOW Global Technologies, Inc.), Appl. WO2004024739, 2004; (*c*) T. R. Boussie, G. M. Diamond, C. Goh, K. A. Hall, A. M. LaPointe, M. K. Leclerc, V. Murphy, J. A. W. Shoemaker, H. Turner, R. K. Rosen, J. C. Stevens, F. Alfano, V. Busico, R. Cipullo and G. Talarico, *Angew. Chem., Int. Ed.*, 2006, **45**, 3278; (*d*) H. W. Boone, K. A. Frazier, D. D. Vanderlende and P. C. Vosejpka (DOW Global Technologies, Inc.), Appl. WO2007037944, 2007; (*e*) K. A. Frazier, R. D. Froese, Y. He, J. Klosin, C. N. Theriault, P. C. Vosejpka, Z. Zhou and K. A. Abboud, *Organometallics*, 2011, **30**, 3318–3329.
7 (*a*) S. Nagy, R. Krishnamurti, J. A. Tyrell, L. V. Cribbs and M. Cocoman (Occidental Chemical Corporation, USA), Appl. WO9633202, 1996; (*b*) S. Nagy, L. N. Winslow, S. Mihan, R. Chevalier, L. Lukesova, I. E. Nifant'ev, P. V. Ivchenko and M. W. Lynch (Equistar Chemicals), Appl. WO2011011041, 2011; (*c*) S. Nagy, L. N. Winslow, S. Mihan, R. Chevalier, L. Lukesova, I. E. Nifant'ev and P. V. Ivchenko (Equistar Chemicals), Appl. WO2011011040, 2011; (*d*) P. P. Fontane and R. L. Kuhlman (Dow Global Technologies), Appl. WO2011102990, 2011; (*e*) S. Nagy, L. N. Winslow, S. Mihan, L. Lukesova, I. E. Nifant'ev, P. V. Ivchenko and V. V. Bagrov (Basell Polyolefine GmbH, Germany), Appl. US 20120016092, 2012; (*f*) S. Song, T. Xiao, L. Wang, C. Redshaw, F. Wang and W.-H. Sun, *J. Organomet. Chem.*, 2012, **699**, 18–25; (*g*) W. Huang, B.-X. Li, Y.-H. Wang, W.-J. Zhang, L. Wang, Y.-S. Li, W.-H. Sun and C. Redshaw, *Catal. Sci. Technol.*, 2011, **1**, 1208; (*h*) M. Lamberti, M. Bortoluzzi, G. Paolucci and C. Pellecchia, *J. Mol. Catal. A: Chem.*, 2011, **351**, 112; (*i*) P. Hu, Y.-L. Qiao, J.-Q. Wang and G.-X. Jin, *Organometallics*, 2012, **31**, 3241.
8 (*a*) F. Cottet, M. Marull, O. Lefebvre and M. Schlosser, *Eur. J. Org. Chem.*, 2003, 1559; (*b*) L. Mao, T. Moriuchi, H. Sakurai, H. Fujii and T. Hirao, *Tetrahedron Lett.*, 2005, **46**, 8419.
9 (*a*) N. Miyaura and A. Suzuki, *Chem. Rev.*, 1995, **95**, 24573; (*b*) A. Suzuki, *Angew. Chem., Int. Ed.*, 2011, **50**, 6722.
10 (*a*) A.-S. Castanet, F. Colobert, P.-E. Broutin and M. Obringer, *Tetrahedron: Asymmetry*, 2002, **13**, 659; (*b*) J. Li, Z. Wang and E. Turner (University Arizona State), Appl. WO2009111299, 2009; (*c*) T. Kaku, S. Tsujimoto, N. Matsunaga, T. Tanaka, T. Hara, M. Yamaoka, M. Kusaka and A. Tasaka, *Bioorg. Med. Chem.*, 2011, **19**, 2428; (*d*) A. Nunez, B. Abarca, A. M. Cuadro, J. Alvarez-Builla and J. J. Vaquero, *Eur. J. Org. Chem.*, 2011, 1280; (*e*) S. K. Nara, H. Nakagawa, Y. Kanda, T. Nakashima, S. Soga, J. Kajita, J.-I. Saito, Y. Shiotsu and S. Akinaga (Kyowa Hakko Kogyo KK), Appl. EP1642880, 2006.
11 (*a*) E. Negishi and S. Baba, *J. Chem. Soc., Chem. Commun.*, 1976, 597; (*b*) E. Negishi and L. Anastasia, *Chem. Rev.*, 2003, **103**, 1979; (*c*) P. Knochel and R. D. Singer, *Chem. Rev.*, 1993, **93**, 2117.
12 (*a*) E. Negishi, F. Luo, R. Frisbee and H. Matsushita, *Heterocycles*, 1982, **18**, 117; (*b*) D. R. Gauthier, R. H. Szumigala, P. G. Dormer, J. D. Armstrong, R. P. Volante and P. J. Reider, *Org. Lett.*, 2002, **4**, 375; (*c*) J. E. Milne and S. L. Buchwald, *J. Am. Chem. Soc.*, 2004, **126**, 13028.
13 U. Scholz and B. Schlummer, *Tetrahedron*, 2005, **61**, 6379.
14 (*a*) U. Zucchini, U. Giannini and E. Albizzati, *J. Organomet. Chem.*, 1971, **26**, 357; (*b*) J. J. Felten and W. P. Anderson, *J. Organomet. Chem.*, 1972, **36**, 87.
15 L. Luconi, A. Rossin, G. Tuci, I. Tritto, L. Boggioni, J. J. Klosin, C. N. Theriault and G. Giambastiani, *Chem.–Eur. J.*, 2012, **18**, 671.
16 F. H. Allen, *Acta Crystallogr., Sect. B: Struct. Sci.*, 2002, **58**, 380.
17 (*a*) R. D. J. Froese, P. D. Hustad, R. L. Kuhlman and T. T. Wenzel, *J. Am. Chem. Soc.*, 2007, **129**, 7831; (*b*) V. Busico, R. Cipulo, R. Pellecchia, L. Rongo, G. Talarico, A. Macchioni, C. Zuccaccia, R. D. J. Froese and P. D. Hustad, *Macromolecules*, 2009, **42**, 4369; (*c*) C. Zuccaccia, V. Busico, R. Cipulo, G. Talarico, R. D. J. Froese, P. C. Vosejpka, P. D. Hustad and A. Macchioni, *Organometallics*, 2009, **28**, 5445.
18 J. C. Chadwick, T. Garoff and J. R. Severn, in *Tailor-Made Polymers*, ed. J. R. Severn and J. C. Chadwick, Wiley-VCH, 2008, p. 43.
19 A. D. Becke, *J. Chem. Phys.*, 1993, **98**, 5648.
20 F. R. Bean and J. R. Johnson, *J. Am. Chem. Soc.*, 1932, **54**, 4415.
21 C. Zimmermann, F. Willig, S. Ramakrishna, B. Burfeindt, B. Pettinger, R. Eichberger and W. Storck, *J. Phys. Chem. B*, 2001, **105**, 9245.
22 M. Schmid, R. Eberhardt, M. Klinga, M. Leskela and B. Rieger, *Organometallics*, 2001, **20**, 2321.
23 C. B. Ziegler and R. F. Heck, *J. Org. Chem.*, 1978, **43**, 2941.
24 L. B. Belykh, N. I. Skripov, L. N. Belonogova, V. A. Umanets, T. P. Stepanova and F. K. Schmidt, *Kinet. Catal.*, 2011, **52**, 702.
25 H. Tomori, J. M. Fox and S. L. Buchwald, *J. Org. Chem.*, 2000, **65**, 5334.
26 G. M. Sheldrick, *SADABS, Program for area detector adsorption correction*, Institute for Inorganic Chemistry, University of Göttingen, Germany, 1996.
27 G. M. Sheldrick, *Acta Crystallogr., Sect. A: Fundam. Crystallogr.*, 2008, **64**, 112.
28 W. W. Yau, "Polyolefin Microstructure Characterization Using 3D-GPC-TREF", TAPPI, 2005 PLACE Conference, 05PLA67.